Journal of Molecular Structure 1216 (2020) 128300

Contents lists available at ScienceDirect

Journal of Molecular Structure

journal homepage: http://www.elsevier.com/locate/molstruc

Spectral, structural, biological and molecular docking studies of a new mixed-valence V(IV)/V(V) ofloxacin complex

Mina Alikhani [a], Mohammad Hakimi [a, *], Keyvan Moeini [a], Mansour Mashreghi [b], Vaclav Eigner [c], Michal Dusek [c]

[a] Chemistry Department, Payame Noor University, 19395-4697, Tehran, I. R., Iran
[b] Department of Biology, Ferdowsi University of Mashhad, Mashhad, 9177948974, I. R., Iran
[c] Institute of Physic of the Czech Academy of Sciences, Na Slovance 2, 182 21, Prague, Czech Republic

ARTICLE INFO

Article history:
Received 24 October 2019
Received in revised form
23 March 2020
Accepted 18 April 2020
Available online 23 April 2020

Keywords:
Ofloxacin
Cyclic tetravanadate anion
Zwitterion
Crystal structure
Antibacterial activity
Docking study

ABSTRACT

In this study, a biologically active mixed-valence V(IV)/V(V) complex $[VO(Hoflo^z)_2(H_2O)][V_4O_{12}]_{0.5}.6H_2O$ (**1**) ($Hoflo^z$ = zwitterionic isomer of ofloxacin) was synthesized by the reaction of $VOSO_4$ with ofloxacin ($Hoflo^z$) in presence of KOH with 1:1:1 ratio. The complex was characterized through the usage of elemental analysis, FT-IR, molar conductivity and single-crystal X-ray diffraction and thermogravimetric analysis (TGA). The results of single crystal X-ray structure determination revealed an ionic structure consisting of $[VO(Hoflo^z)_2(H_2O)]^{2+}$ and $[V_4O_{12}]^{4-}$ units with 1:0.5 stoichiometry. The V^{+4} ion in the cationic unit has octahedral geometry while each V^{+5} ion of the eight-member cyclic tetravanadate anion is tetrahedrally coordinated. In regards to the crystal structure of **1**, the bidentate ofloxacin ligand is coordinated to the V^{+4} ion in its zwitterionic form ($^+HN-\cdots-COO^-$) through the oxygen atoms of the pyridone and carboxylato groups. The thermodynamic stability of two isomeric forms of Hoflo and **1** along with their charge distribution patterns was studied by DFT and NBO analysis. Also, the ability of the ligand to interact with ten selected biomacromolecules (BRAF kinase, CatB, DNA gyrase, HDAC7, rHA, RNR, TrxR, TS, Top II and B-DNA) was investigated by docking calculations. These studies revealed that this ligand can bind to the proteins and DNA molecule and could be consider as biologically active compound. Finally, the antibacterial activities of the free Hoflo ligand and its vanadium complex have been evaluated against *Escherichia coli* (*E. coli*) and *Staphylococcus aureus* (*S. aureus*) strains through the utilization of broth microdilution and well diffusion methods. The complex showed antibacterial effect similar to the free Hoflo ligand on the selected bacterial strains and these compounds were more active against Gram-negative bacteria.

1. Introduction

Quinolones (quinolonecarboxylic acids or 4-quinolones) are known as a very important family of the synthetic antibacterial drugs that are prescribed in great extent for the treatment of different bacterial diseases. Recently, the synthesis of novel quinolone analogues with increased activity and potential for being applied throughout the treatment of various bacterial diseases has been considered [1]. Ofloxacin is a member of this large family (Hoflo, Fig. 1) that is widely used to treat bacterial infections that cause bronchitis, pneumonia, chlamydia, gonorrhea, skin infections, urinary tract infections, and infections of the prostate [2]. While containing a zwitterionic form (Fig. 1), Ofloxacin usually acts as bidentate ligand due to the oxygen atoms of pyridone and carboxylate groups [3]. The existence of interaction between quinolones and metal ions stands as the subject of active research in bioinorganic chemistry [4].

Nowadays, synthetic antibacterial drugs such as quinolones are often detected in the form of inorganic coordination compounds. Next to being capable of increasing their solubility, the drugs that come in the form of metal complexes possess modified toxicological and pharmacological properties which has consequently caused their synthesis to be of importance [5]. It was found that quinolones have a similar affinity for the metal ions, forming chelates more stable with hard Lewis acids like the trivalent cations (Al^{3+}, Fe^{3+}). Chelates less stable are formed with the cations of

* Corresponding author.
E-mail address: mohakimi@yahoo.com (M. Hakimi).

https://doi.org/10.1016/j.molstruc.2020.128300
0022-2860/

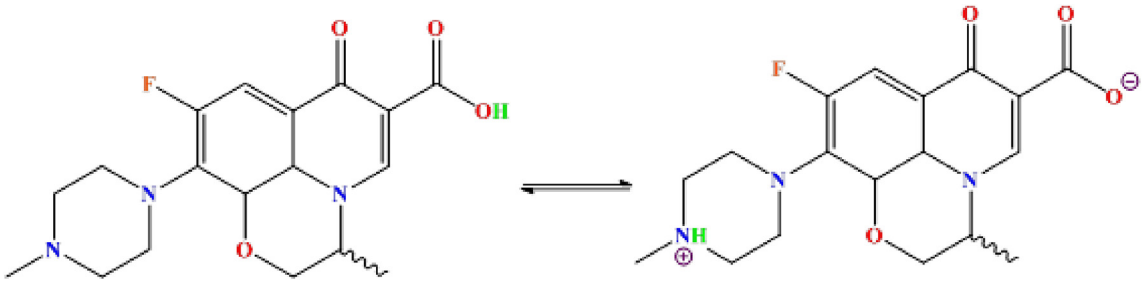

Fig. 1. Molecular structure of Hoflo (left) and its zwitterion form (right).

group 2 A (Mg^{2+}, Ca^{2+}, Ba^{2+}) [6].

According to the literature review, there are several reports on the synthesis of ofloxacin complexes with Mg^{+2} [7], Fe^{2+} [8], Ru^{2+} [9], Co^{2+} [10], Ni^{2+} [11], Pt^{2+} [12], Cu^{2+} [13] and Zn^{2+} [14] and investigation of their applications. Since there are no reports of the synthesis of ofloxacin complexes with vanadium, in the present work, we report the first example of a oxidovanadium complex with ofloxacin.

In recent years, the coordination chemistry of oxidovanadium complexes have been considered for their role in catalytic activities since they contain a vital functionality throughout a variety of biochemical processes such as haloperoxidation [15], phosphorylation [16], insulin-mimicking [17], nitrogen fixation [18], tumor growth inhibition, and prophylaxis against carcinogenesis [19]. Moreover, high-valence vanadium complexes have been investigated as new versatile catalytic reagents for a wide range of oxidation reactions [20], such as the oxidation of olefins and alcohols [21,22], benzene/alkyl aromatic compounds, and sulfides [23]. Also, it is noticeable that the complexation of vanadium with organic ligands minimizes unfavorable effects of its inorganic salts without sacrificing important benefits [24].

Herein we describe the synthesis, characterization and crystal structure of a new oxidovanadium complex, $[VO(Hoflo^{z})_2(H_2O)][V_4O_{12}]_{0.5}.6H_2O$ (**1**), containing Zwitterionic form of ofloxacin ligand ($Hoflo^{z}$) and a cyclic eight-membered tetravanadate anion ($[V_4O_{12}]^{4-}$). For the study of the thermodynamic stability and charge distribution patterns of ligand and complex, DFT and NBO analyses were performed, respectively.

To evaluate the biological activities of Hoflo and $Hoflo^{z}$, docking calculations were run to investigate the possibility of an interaction between these compounds and ten biomacromolecular targets [25–29], as the following: BRAF kinase, Cathepsin B (CatB), DNA gyrase, Histone deacetylase (HDAC7), recombinant Human albumin (rHA), Ribonucleotide reductases (RNR), Thioredoxin reductase (TrxR), Thymidylate synthase (TS), Topoisomerase II (Top II) along with B-DNA. These proteins were selected either due to their reported roles in cancer growth or as transport agents that can effect drug pharmacokinetic properties (e.g., rHA). The DNA gyrase was included to study the possibility of anticancer properties and their activity as antimalarial agents [30]. The knowledge gained from docking on the B-DNA should be useful for the development of potential probes in regards to DNA structure and new therapeutic reagents for tumors and other diseases [31]. Additionally, the antimicrobial activity of the Hoflo and **1** was investigated by determining the minimum inhibitory concentration (MIC) and measuring the diameter inhibition zone against Gram-positive *S. aureus* (ATCC 25923) and Gram-negative E. *coli* (ATCC 25922) microorganisms.

2. Experimental

2.1. Materials and instrumentation

All of the chemicals, solvents, and ofloxacin drug (purity: 99.7%) for synthesis and analysis were purchased from Sigma Aldrich company. Infrared spectra as a KBr disk in the 4000–500 cm^{-1} region were recorded at room temperature by the employment of a Shimadzu FT-IR 8400 spectrometer. Carbon, hydrogen, and nitrogen contents were determined through a Thermo Finnigan Flash Elemental Analyzer 1112 EA, while the attained results were in agreement with the calculated values. The molar conductivity of the complex was prepared in DMF (1.0×10^{-3} mol/L) and measured using a Herisau Metrohm model CH-9101. The TGA was measured with an SDT Q600-TA instruments under an oxygen atmosphere with a heating rate of 10 °C/min in the temperature span of 25–1000 °C.

2.2. Preparation of $[VO(Hoflo^{z})_2(H_2O)][V_4O_{12}]_{0.5}.6H_2O$

A mixture of $VOSO_4$ (0.163 g, 1 mmol), ofloxacin (0.361 g, 1 mmol) and water (15 mL) was adjusted to pH 7 with KOH (1 M) solution and refluxed for 2 h. Then, the reaction mixture was cooled to room temperature and subsequent to days, the yellow prismatic crystals have been collected by filtration, washed with water and dried in air. mp: 300 °C. Yield: 70%. Molar conductivity (1×10^{-3} mol L^{-1}; DMF): 92 $\Omega^{-1}cm^2$ mol^{-1}. Elemental analysis: $C_{36}H_{46}F_2N_6O_{22}V_3$ (1105.6); Calculate: C, 41.51; H, 4.45; N, 8.07%; Found: C, 41.15; H, 4.95; N, 7.67%. IR (KBr disc, cm^{-1}): 3402 m (ν O–H)$_{water}$, 3352 w (ν N–H), 2929 w (ν_{as} CH_2), 2819 w (ν_s CH_2), 1610 s (ν C=O)$_{pyridone}$, 1580 s (ν_{as} COO), 1488 s (ν C=C), 1382 s (ν_s COO), 1256 s (ν C–O), 1186 w (ν C–N), 954 s (ν V=O), 750 (ν_{as} V–O–V), 640 s (ν_s V–O–V), 550 w (ν V–O).

2.3. Structure determinations

Suitable single crystal of the dimensions $0.12 \times 0.09 \times 0.03$ mm was chosen for X-ray diffraction study. Crystallographic measurements were done at 95 K with using a Super-Nova diffractometer equipped with a micro-focus sealed tube, mirror-collimated Cu Kα radiation ($\lambda = 1.54184$ Å), and a CCD detector (Atlas S2). Thereafter, the structure was solved with the charge flipping algorithm by Superflip [32] and refined by full-matrix least-squares on F2 using program Jana2006 [33]. All hydrogen atoms present in the structure model were discernible in difference Fourier maps and could be refined to reasonable geometry. According to common practice H atoms bonded to C were kept in ideal positions with C–H = 0.96 Å while positions of H atom bonded to N and O were

refined with restrained bond lengths. In both cases, U_{iso}(H) was set to 1.2U_{eq} (C, N, O). All non-hydrogen atoms were refined using harmonic refinement. The hydrogen atoms of four water molecules could not be located in difference Fourier maps and therefore are absent in the structure model. MCE software [34] was used for visualization of difference Fourier maps. Diagrams of the molecular structures and unit cells were created using Diamond software [35].

2.4. Computational details

All structures were optimized with the Gaussian 09 software [36] and calculated for an isolated molecule using Density Functional Theory (DFT) [37] at the B3LYP [38]/6-31G [39] (d,p) level of theory for ligand and its Zwitterionic form and B3LYP/LanL2DZ [40] for complex and NBO analysis. The X-ray structural data of complex **1** was used as input for the theoretical calculations. The structure of the ligand was extracted from the cif file of the complex **1** and used for DFT studies.

2.5. Docking studies

We obtained the pdb files of 4r5y, 3ai8, 5cdn, 3c0z, 2bx8, 1peo, 3qfa, 1njb, 4gfh, 1bna for the ten receptors including BRAF kinase, Cathepsin B (CatB), DNA gyrase, Histone deacetylase (HDAC7), recombinant Human albumin (rHA), Ribonucleotide reductases (RNR), Thioredoxin reductase (TrxR), Thymidylate synthase (TS), Topoisomerase II (Top II), B-DNA, respectively, from the Protein Data Bank (pdb) [41]. The full version of Genetic Optimisation for Ligand Docking (GOLD) 5.5 [42] was used for the docking studies. The Hermes visualizer in the GOLD Suite was applied to further prepare the ligand, complex, and receptors for docking, while the optimized structure of ligands was used for the docking studies. The region of interest used for GOLD docking was defined as all of the protein residues within 6 Å of the reference ligand "A" that had accompanied the downloaded protein. In regards to B-DNA, the region of interest was defined on DNA backbone within 10 Å of the O2, DT19 atoms for minor grooves. All the free water molecules that exist within the structure of proteins were deleted before docking. All the other parameters were applied in default values and the compounds were submitted to ten genetic algorithm runs through the GOLDScore fitness function.

2.6. Antibacterial activities

The antibacterial activities of Hoflo ligand and **1** were investigated *in vitro* against the bacterial species Gram-positive *S. aureus* (ATCC 25923) and Gram-negative E. *coli* (ATCC 25922). Initially, compounds were dissolved in dimethylsulfoxide (DMSO) and the antibacterial activities of all solutions were determined by broth microdilution and well diffusion methods. To proceed with these methods, bacterial strains were grown in a nutrient medium at 37 °C overnight to obtain a cell count of approximately 10^8 CFU/mL.

2.6.1. Measurement of minimum inhibitory concentration (MIC)

The MIC values were studied for bacterial species using a microtiter plate method. For this test, 70 μl of the bacterial suspension containing 10^8 CFU/mL were added to 70 μl of the compounds dispersed in DMSO. Then, we have appended 70 μl of nutrient broth medium to each well of the microtiter plate. To finish the process, after three intervals, dilution concentrations of 4, 8, 16, 32, 64 μg/mL of the compounds were produced in each plate. Optical density (OD) of all concentrations was measured at zero, as well as subsequent to 18 h of incubation at 37 °C.

2.6.2. Disc diffusion method

In this method, the compounds were dissolved in DMSO solvent until reaching the final concentrations of 4, 8, 16, 32, 64 μg/mL and were sterilized through autoclaving. Thereafter, cell concentrations of all test microorganisms were required to be adjusted at 0.5 McFarland (10^8 CFU/mL) and by the of sing sterile swabs, each

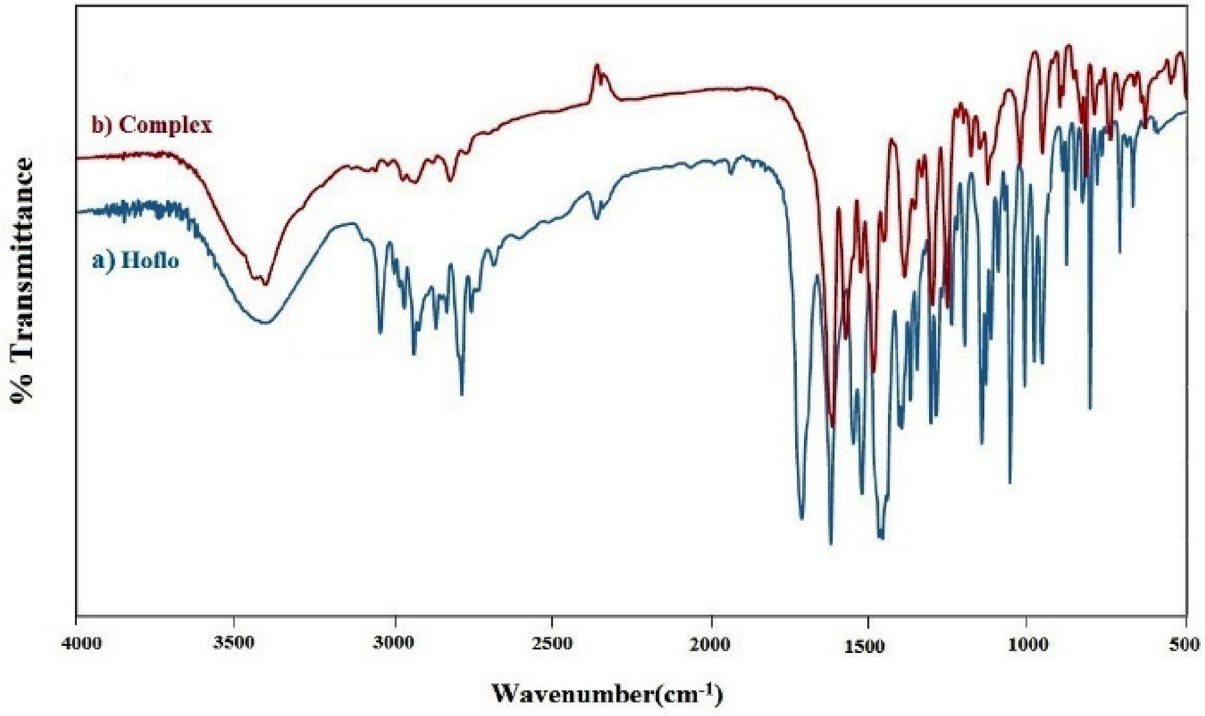

Fig. 2. The IR spectra of (a) Hoflo, (b) $[VO(Hoflo^z)_2(H_2O)][V_4O_{12}]_{0.5}$.$6H_2O$ in KBr pellet.

Table 1
Crystal data and data collection, refinement parameters for complex **1**.

Empirical formula	$C_{36}H_{42}F_2N_6O_{10}V{\cdot}0.5(V_4O_{12}){\cdot}2(H_2O){\cdot}4(O)$
Formula weight (g mol^{-1})	1105.6
Crystal size (mm^3)	0.12 × 0.09 × 0.03
T (K)	95
Crystal system	Triclinic
Space group	*P*-1
a (Å)	9.3623 (4)
b (Å)	13.8516 (7)
c (Å)	18.7684 (9)
α (°)	99.467 (4)
β (°)	97.344 (3)
γ (°)	101.761 (4)
V ($Å^3$)	2317.3 (2)
Z	2
ρ_{calc}, (g cm^{-3})	1.585
μ (mm^{-1})	5.83
F (000) (e)	1134
θ range for cell measurement (°)	3.7–74.1
h, k, l ranges	$-11 \le h \le 11$, $-17 \le k \le 17$, $-23 \le l \le 23$
Reflections measured, independent	50358, 15842
Parameters, restrains	651, 11
R_{int}	0.1097
Reflections with $I > 3\sigma(I)$	8945
R ($F^2 > 3\sigma(F^2)$)	0.072
wR (F^2)	0.165
$\Delta\rho_{max}$, $\Delta\rho_{min}$ (e $Å^{-3}$)	0.80, −0.58

microbial suspension was inoculated on nutrient agar. As the last step, filter paper discs (6 mm in diameter) were placed on the agar surface, and 50 μl of the test samples were pipetted into the discs. After 24 h of incubation at 37 °C, the diameters of inhibition zones (DIZ) are measured in millimetres (mm).

3. Results and discussion

3.1. IR spectroscopy

The FT-IR spectrum, summarized in the experimental section, is focused on the functional groups of carboxylate and pyridone groups. The observed broad absorption band at 3402 cm^{-1} region in regards to **1** refers to the O–H stretching vibration of water molecules [43,44]. In the FT-IR spectrum of free Hoflo (Fig. 2 (a)), The band appears at 3352 cm^{-1}, for ν (N–H) of the NH_2^+ group, showing the Hoflo ligand is in a neutral zwitterionic form ($^+$HN–···–COO^-) [45]. Furthermore, three bands at 1640, 1620, and 1400 cm^{-1} are assigned to the ν (C=O) vibrations of the pyridone group, as well as the ν_{as} (COO) and ν_s (COO) of the carboxylate group, respectively [46]. After complexation (Fig. 2 (b)), the ν (C=O), ν $(COO)_{as}$, ν $(COO)_s$ are shifted 30, 40 and 18 cm^{-1} to the lower frequencies. Also, the difference of Δ [$= \nu_{asym}$ (C=O) $-\nu_{sym}$ (C=O)] is used to measure the coordination of carboxylate ligands, and the difference (Δ) of this complex has been measured to be 198 cm^{-1}, which is suggestive of an asymmetric monodentate carboxylate

Table 2
Selected bond lengths (Å) and valence angles (°) of complex **1**.

Distances			
V1–O3a	1.993 (3)	V1–O4a	2.203 (3)
V1–O3b	1.977 (4)	V1–O4b	2.003 (4)
V1–O1v	1.619 (4)	V1–O2v	2.031 (4)
V2–O1	1.810 (5)	V2–O2	1.797 (4)
V2–O3	1.626 (4)	V2–O4	1.650 (4)
V3–O1	1.823 (5)	V3–$O2^i$	1.787 (4)
V3–O5	1.632 (4)	V3–O6	1.650 (5)
Angles			
O3a–V1–O4a	81.01 (13)	O3a–V1–O3b	163.16 (14)
O3a–V1–O4b	87.84 (14)	O3a–V1–O1v	97.26 (17)
O3a–V1–O2v	89.36 (15)	O4a–V1–O3b	82.33 (13)
O4a–V1–O4b	82.78 (14)	O4a–V1–O1v	176.58 (18)
O4a–V1–O2v	82.84 (14)	O3b–V1–O4b	87.65 (14)
O3b–V1–O1v	99.51 (16)	O3b–V1–O2v	90.99 (15)
O4b–V1–O1v	100.14 (18)	O4b–V1–O2v	165.61 (15)
O1v–V1–O2v	94.21 (18)		
O1–V2–O2	108.4 (2)	O1–V2–O3	107.2 (2)
O1–V2–O4	111.8 (2)	O2–V2–O3	113.85 (19)
O2–V2–O4	106.63 (19)	O3–V2–O4	109.1 (2)
O1–V3–$O2^i$	110.82 (19)	O1–V3–O5	110.1 (2)
O1–V3–O6	107.1 (2)	$O2^i$–V3–O5	110.2 (2)
$O2^i$–V3–O6	108.9 (2)	O5–V3–O6	109.7 (2)

Symmetry codes: (i) $-x+1$, $-y+1$, $-z+1$.

Table 3
Selected Hydrogen bond geometry, lengths (Å) and valence angles (°) of complex **1**.

D–H···A	*d* (D–H)	*d* (H···A)	*d* (D···A)	< (DHA)
O2v–H1o2v···O1a^{i}	0.860 (9)	2.12 (2)	2.935 (6)	159 (4)
O2v–H2o2v···O9	0.86 (3)	1.97 (3)	2.575 (5)	126 (5)
O7–H1o7···O2b	0.86 (5)	2.03 (5)	2.827 (6)	153 (4)
O7–H2o7···O2a^{ii}	0.86 (5)	2.02 (5)	2.846 (6)	162 (4)
O8–H1o8···O5	0.86 (5)	1.97 (6)	2.808 (7)	166 (5)
O8–H2o8···O3^{iii}	0.86 (3)	2.46 (5)	3.023 (6)	124 (5)
N3a–H1n3a···O1^{iv}	0.92 (5)	1.93 (5)	2.774 (6)	151 (4)
N3b–H1n3b···O4^{i}	0.92 (5)	1.93 (5)	2.822 (7)	162 (5)

Symmetry codes: (*i*) -*x*, -*y*+1, -*z*; (*ii*) *x*+1, *y*, *z*; (*iii*) -*x*+1, -*y*+1, -*z*+1; (*iv*) -*x*+1, -*y*+1, -*z*.

[47]. The attachment of an oxo ligand to the vanadium (IV) ion proves by a band at 954 cm^{-1}. Also, the asymmetric and symmetric vibrations of the bridged V–O–V bonds of the cyclic tetravanadate anion are observed at 640 and 750 cm^{-1} [48]. Finally, a weak band at 550 cm^{-1} is attributed to the metal-ligand stretching vibration (V–O) [49].

3.2. Description of crystal structure

Crystallographic data and refinement details are given in Table 1. In addition, selected bond lengths, angles and hydrogen bond geometries are shown in Table 2 and Table 3.

3.2.1. Crystal structures of $[VO(Hoflo^{z})_2(H_2O)]$ $[V_4O_{12}]_{0.5}.6H_2O$

Single crystal X-ray analysis reveals an ionic complex (Fig. 3) that crystallized in the Triclinic space group *P*-1. The asymmetric unit is consisted of a coordinated cation $[VO(Hoflo^{z})_2(H_2O)]^{2+}$, half of the cluster anion $[V_4O_{12}]^{4-}$ and six crystal water molecules. To the best of our knowledge, this is the first example regarding the crystal structure of an oxidovanadium complex with ofloxacin ligand. In the cationic unit, the coordination geometry around the vanadium (IV) is distorted octahedral geometry with VO_6 environment. Each of the $Hoflo^{z}$ molecules is bonded to the vanadium atom in the bidentate mode through the O3 oxygen atom of the carboxylate group and O4 oxygen atom from the pyridone group. Also, two ligands have *cis* position and are in a zwitterionic form ($^{+}$HN–···–COO^{-}) with the protonation of the terminal piperazinyl nitrogen atom (N3). In addition of two $Hoflo^{z}$ ligands, the octahedral geometry around the vanadium atom is completed by coordination of an oxo ligand along with a water molecule. Among the different coordinated bond lengths, the $V{=}O^{oxo}$ and $V–O^{pyridone}$ which have a *trans* position are the shortest and longest ones. The $Hoflo^{z}$ ligand has one chiral center on the carbon atom (C9a and C9b), and each cationic units contains two chiral centers with similar enantiomeric form. Although **1** has two chiral centers, the crystals are a racemic mixture of *R*, *R* and *S*, *S* isomers in alternate layers [50,51]. A study of the Cambridge Structural Database (CSD) [52] revealed that free ligand does not exist in the zwitterionic form [53], which could be related to the fact that the thermodynamic stability of Hoflo is higher than $Hoflo^{z}$. This observation is studied by DFT studies in the theoretical section. Based on the CSD data, in addition to the zwitterionic form, this ligand can form a cationic H_2oflo^{+} [54], and an anionic Hoflo [55] units, while being capable of functioning as bidentate OO-donor ligand as well.

A cluster anion ($[V_4O_{12}]^{4-}$) contains four corner-sharing [VO_4] tetrahedra (Fig. 4), each of them including two O bridge atoms and two O terminal atoms. The bond lengths average of $(V–O)^{bridge}$ is by 0.164 Å longer than the $(V–O)^{terminal}$ average.

In the crystal structure of **1** (Fig. 4), there are intermolecular O–H···O and N–H···O hydrogen bonds. The latter of them appears to have a larger impact on the crystal structure, which results in forming an infinite chain in the direction of [1 0 0]. The O–H···O hydrogen bonds either hold the chains together, or act as a bridge of complex anion oxygen atoms. These interactions form motifs with graph-set notations including $D^1_1(2)$, $R^2_2(20)$, $R^2_2(18)$, $R^2_2(19)$, $R^2_2(14)$, $R^2_2(15)$, $R^4_4(56)$, $R^2_1(4)$ and $R^2_2(8)$. Hydrogen atoms of four water molecules could not be located in difference Fourier maps,

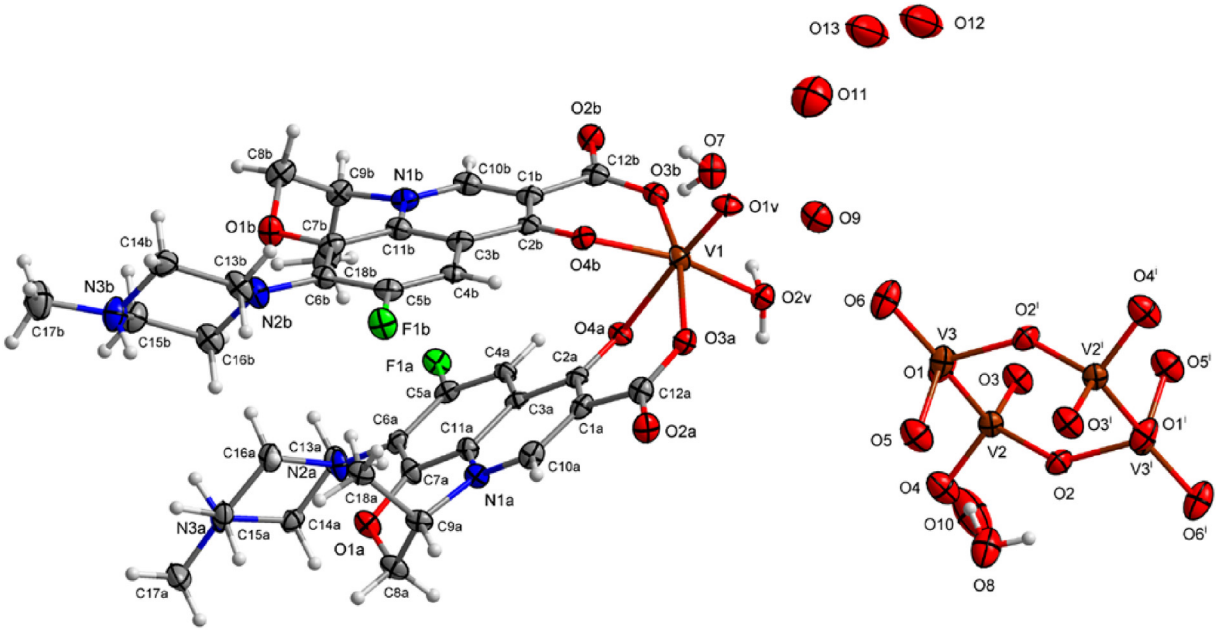

Fig. 3. Diagram of $[VO(Hoflo^{z})_2(H_2O)][V_4O_{12}]_{0.5}.6H_2O$ complex ADPs, presenting the selected atoms labelled and ellipsoids at 30% of probability. Symmetry code: (*i*) -*x*+1, -*y*+1, -*z*+1.

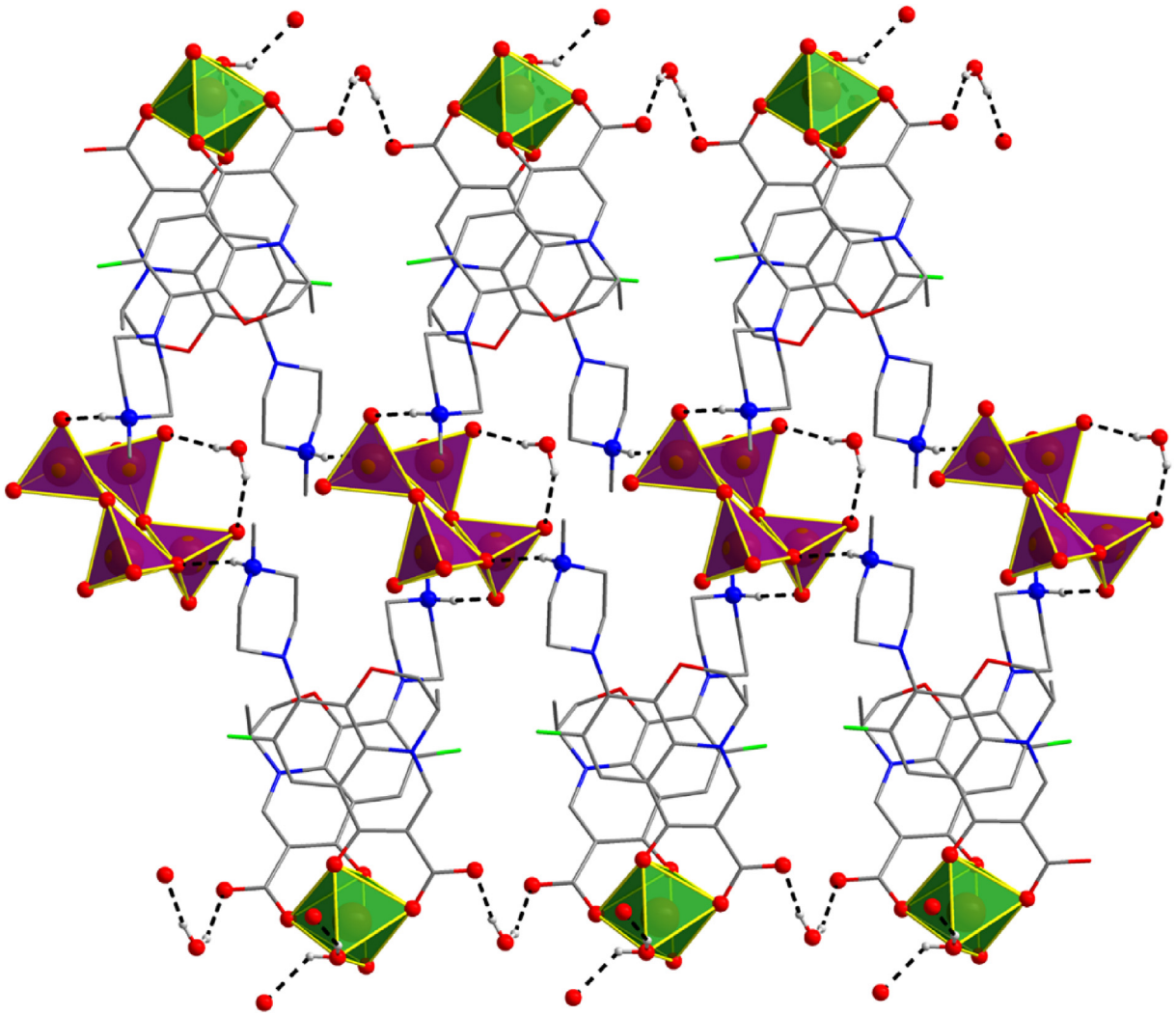

Fig. 4. A view of coordination polyhedral and hydrogen bonds of $[VO(Hoflo^{z})_2(H_2O)][V_4O_{12}]_{0.5}.6H_2O$. Octahedral depicted in green and tetrahedral in purple. Hydrogen atoms not involved in hydrogen bonds were omitted for clarity.

therefore their involvement in hydrogen bonding will not be discussed.

3.3. Thermal Analysis

Thermal gravimetric analysis (TGA) was performed to study the thermal stability of **1** between 25 and 1000 °C under oxygen flow (Fig. S1). The TGA curve of **1** showed two decomposition steps. The first decomposition step occurred in the 350–520 °C temperature range with a weight loss of 42.46% due to the loss of six coordinated of waters and Hoflo ligand. The second stage of decomposition occurred in the 520–750 °C temperature range with a weight loss

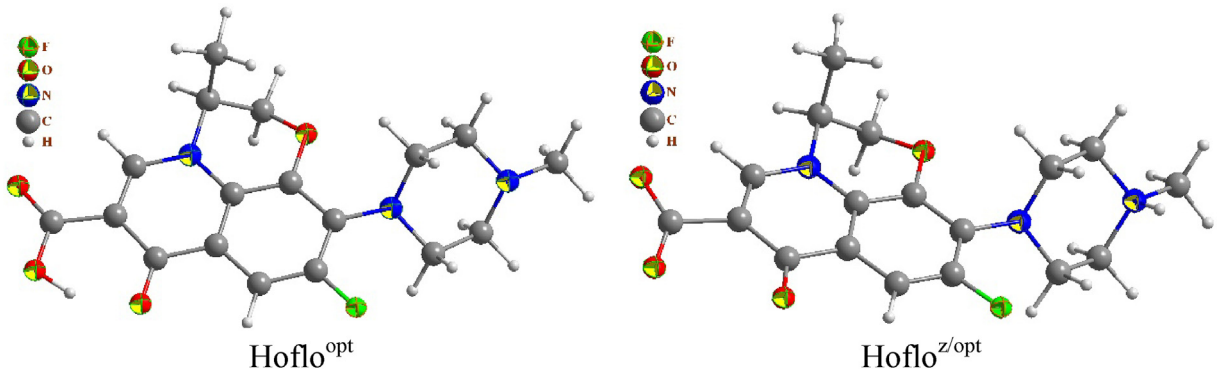

Fig. 5. Optimized structures of the $Hoflo^{opt}$ and $Hoflo^{z/opt}$.

Table 4
The NBO analysis results for optimized ligand and complex **1**. The values are the average charge on similar atoms.

	$C(sp^2)$	$C(sp^3)$	C^F	C^{carbo}	C^{COO}	$H(C\text{-}sp^2)$	$H(C\text{-}sp^3)$	H^N	H^{water}	N	O^{ether}	O^{carbo}	O^{COO}	O^{oxo}	O^{water}	F	V
$Hoflo^{opt}$	−0.02	−0.31	0.40	0.50	0.81	0.27	0.24	–	–	−0.45	−0.53	−0.64	−0.67	–	–	−0.33	–
$Hoflo^{z/opt}$	−0.02	−0.31	0.37	0.45	0.73	0.28	0.26	0.46	–	−0.46	−0.57	−0.56	−0.73	–	–	−0.36	–
$\mathbf{1}^{opt}$ (cationic)	0.02	−0.25	0.40	0.50	0.84	0.27	0.24	0.46	0.55	−0.49	−0.60	−0.59	−0.66	−0.32	−0.88	−0.38	0.83
$\mathbf{1}^{opt}$ (anionic)	–	–	–	–	–	–	–	–	–	–	(Bridging O) −0.65		(Terminal O) −0.61		–	–	0.87

of 34.31%, corresponding to the loss of lattice water and Hoflo ligand. The percentage of the final metal oxide (V_2O_5) residue of **1** was calculated from the weight of the ash obtained.

3.4. Theoretical studies

In order to compare the theoretical and the solid-state structure of **1**, DFT calculations were performed for an isolated molecule. In regards to complex **1**, the cationic ($[VO(Hoflo^z)_2(H_2O)]^{2+}$) and anionic ($[V_4O_{12}]^{4-}$) units were separately optimized. In addition to the Hoflo ligand, its Zwitterion isomer that is known as $Hoflo^z$, was optimized as well (Fig. 5).

Similarly, as in the solid state, in the octahedral geometry of vanadium atom in the cationic moiety of $\mathbf{1}^{opt}$, the longest and shortest coordinated bond lengths have *trans* position to each other and piperazine rings are in chair conformation. The dihedral angle between mean planes through two six-membered chelate rings with the *cis* position in $\mathbf{1}^{opt}$ and **1** is detected to be 73.19 and 54.27°, respectively, confirming that the octahedral geometry of vanadium atom in the gaseous state is closer to an ideal octahedron. Regarding the optimized structures of $Hoflo^{opt}$ and $Hoflo^{z/opt}$, the piperazine rings have chair conformation and the dihedral angle

Table 5
HOMO and LUMO orbitals for $Hoflo^{opt}$ ligand and its Zwitterion isomer ($Hoflo^{z/opt}$) along with cationic and anionic moieties of $\mathbf{1}^{opt}$.

	LUMO	HOMO
$Hoflo^{opt}$	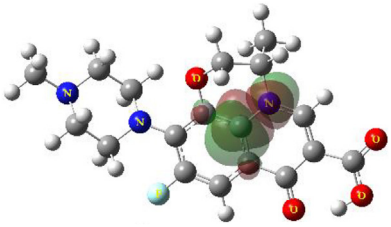	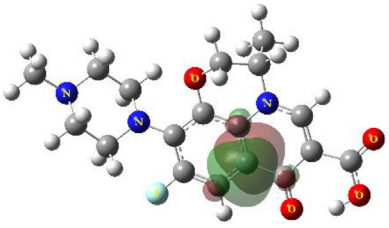
$Hoflo^{z/opt}$	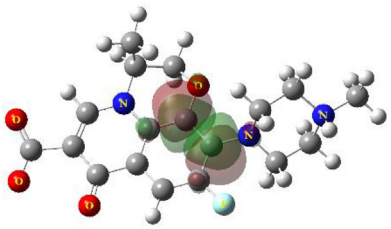	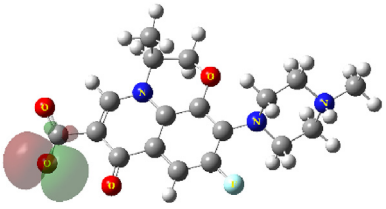
$\mathbf{1}^{opt}$ (cationic)	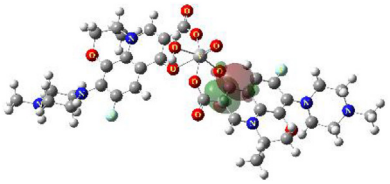	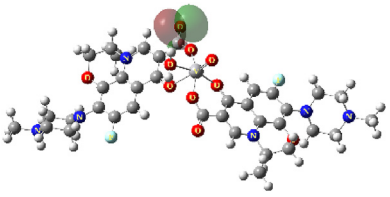
$\mathbf{1}^{opt}$ (anionic)	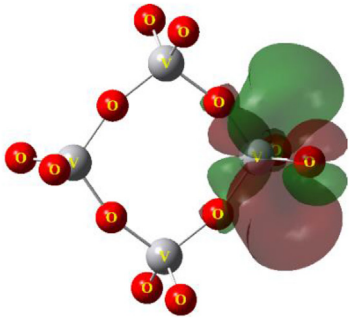	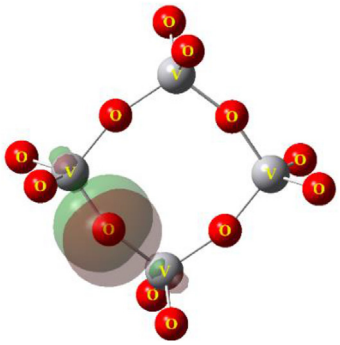

Table 6
The calculated fitness values for optimized ligand and its Zwitterion isomer along with Doxorubicin drug.

	B-DNAs/Min	BRAF-kinase	CatB	DNA-gyrase	HDAC7	rHA	RNR	TrxR	TS	Top II
$Hoflo^{opt}$	55.98	48.76	29.50	49.88	53.89	51.84	39.53	51.24	42.87	46.53
$Hoflo^{z/opt}$	58.03	46.81	31.80	49.40	53.53	49.93	39.32	50.60	44.50	47.78
Doxorubicin	83.10	54.21	25.95	52.97	50.73	50.10	49.18	66.70	53.34	59.05

between mean planes through the piperazine and cyclohexane rings is 44.87 and 54.40°, respectively in $Hoflo^{opt}$ and $Hoflo^{z/opt}$, confirming that the piperazine ring inclines to be perpendicular to the cyclohexane ring.

An NBO analysis was performed to study the charge distribution pattern of $Hoflo^{z/opt}$ ligand before and after complexation (Table 4). In cationic and ionic parts of $\mathbf{1}^{opt}$, the calculated charge on the metal atoms ($V^{cationic}$: +0.83, $V^{anionic}$: +0.87) is lower than the formal charge ($V^{cationic}$: +4, $V^{anionic}$: +5) owing to the electron donation of the ligand upon complexation. These calculations reveal that in the cationic moiety and among the different atoms, the charges on the carbon atoms and oxygen atoms of the carboxylate group are significantly positive compared to the free ligand ($Hoflo^{z/opt}$), indicating that these atoms play an important role in electron donation toward the metal atom and in decreasing its charge. The charge on oxo ligand is calculated to be −0.32 which is by +1.68 more positive than its formal charge (−2), confirming the high electron donation ability of this ligand toward metal ion. There are two types of oxo ligands in the anionic portion that includes the bridging and the terminal one. According to the NBO analysis, the electron donation of terminal oxo ligands is slightly (+0.04) higher than that of the bridging ones. In addition, the comparison between charge patterns of two isomeric forms of ligand revealed that the charge on the carbon and oxygen atoms of the carboxylate group of $Hoflo^{opt}$ is significantly more positive than the $Hoflo^{z/opt}$ due to the proton transfer from ammonium group to the carboxylate. Based on the optimisation results, the thermodynamic stability of the $Hoflo^{opt}$ is by −87.8 kcal/mol higher than in its zwitterion isomer. In the optimized structure of the ligand and its isomer, the existence of certain C-sp^2 atoms is quiet significant throughout the formation of frontier orbitals (Table 5). Also, the oxygen atoms of the carboxylate group have a significant quota in the HOMO orbital of

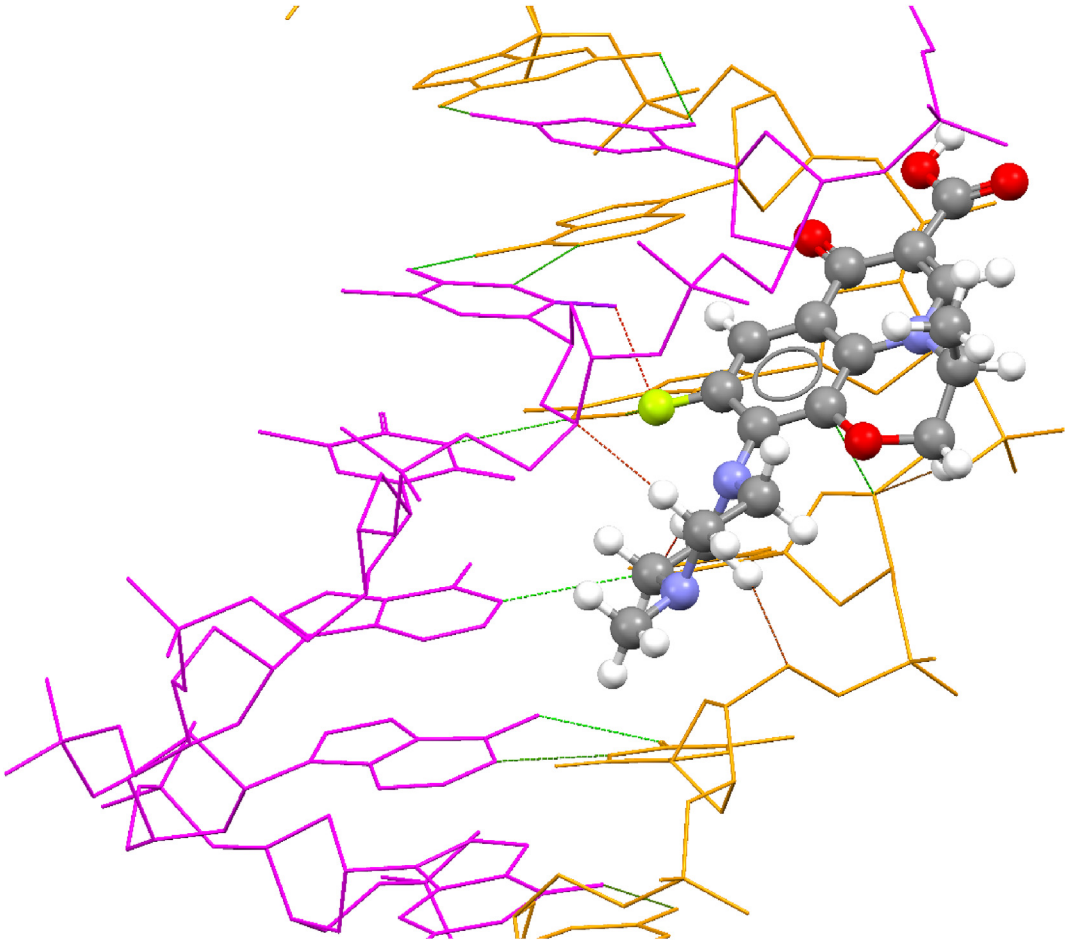

Fig. 6. Docking study results, showing the interaction between the $Hoflo^{opt}$ and B-DNA (minor groove).

Hoflo$^{z/opt}$. In the case of cationic unit of **1**^{opt}, the LUMO and HOMO orbitals are delocalized on the carbon atom of the carbonyl group and the oxo ligand, respectively (Table 5). In the anionic moiety of **1**^{opt}, one of the V(O^{terminal})$_2$ units forms LUMO and one of the bridging oxo ligand forms HOMO orbital.

3.5. Docking studies

For the purpose of predicting the biological activities of the Hoflo^{opt} ligand and its isomer Hoflo$^{z/opt}$, interactions of these compounds with ten macromolecular receptors were investigated by the application of GOLD docking software. The GOLD docking results are reported in terms of the values of fitness, where the higher fitness value are defined better docking interaction of the compound [25–29,56,57]. The docking outcomes presented in this work are the best binding results out of ten favourites predicted by GOLD. Additionally to evaluate the calculated fitness values, these scores were compared with those of the anti-cancer drug doxorubicin (a cancer medication that interferes with the growth and spread of cancer cells in the body [25]).

As it can be observed in GOLD docking prediction (Table 6), the two studied structures could be considered as biologically active compounds and based on the calculated values, the best-predicted target for titled compounds is HDAC7. Docking calculations revealed that the studied compounds have higher fitness values than the doxorubicin in binding toward the CatB, HDAC7 and rHA (only Hoflo^{opt}). Docking studies also revealed that all studied compounds could be placed in the minor grooves of a DNA molecule, which label these compounds and their complexes as a suitable choice for DNA binding studies. Also, the ligand in its zwitterion form shows the better binding ability to the DNA. The docking results of the interaction between Hoflo^{opt} and Hoflo$^{z/opt}$ with B-DNA (minor grooves) are shown in Figs. 6 and 7, respectively.

3.6. Biological activity

The efficiencies of Hoflo ligand and its complex was tested against one Gram-positive (*S. aureus*) and a Gram-negative (*E. coli*) microorganisms by determining the minimum inhibitory concentration (MIC) and measuring the diameter inhibition zone. The MIC values of compounds are represented in Table 7. The MIC values of the ligand and the complex were 4 μg/mL against *E. coli* and 32 μg/mL against *S. aureus*. The results showed that these compounds were more active against Gram-negative bacteria. We also investigated the antibacterial activity of vanadyl sulfate at the applied

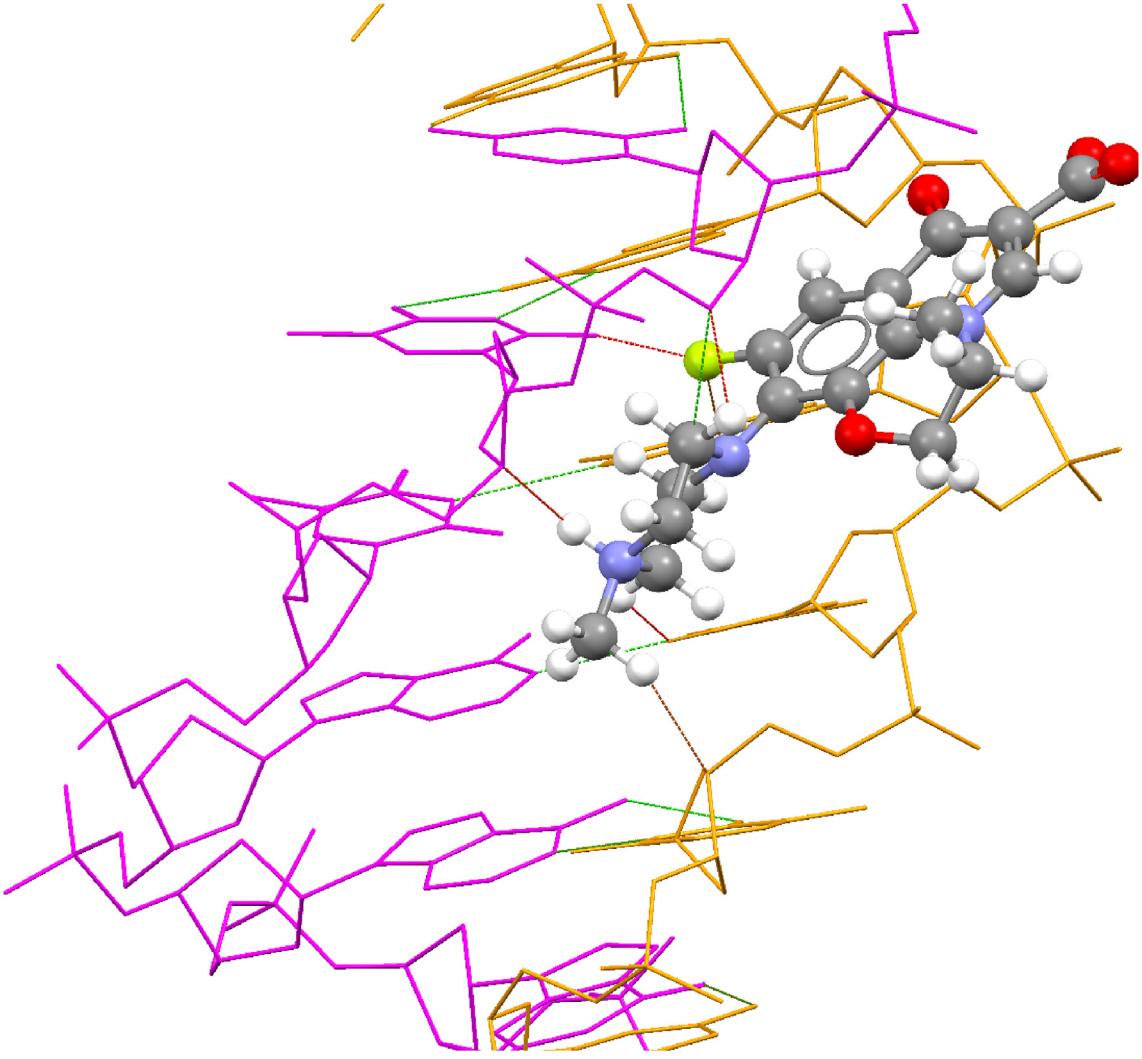

Fig. 7. Docking study results, showing the interaction between the Hoflo$^{z/opt}$ and B-DNA (minor groove).

Table 7
Antimicrobial activities of free ligand and complex evaluated by minimum inhibitory concentration (MIC).

Compound	*E. coli* MIC	*S.aureus* MIC
Hoflo	4	32
Complex **1**	4	32

concentration of the complex and detected zero antibacterial effects at this concentration. Antibacterial activity of quinolones and their complexes has been assessed in previous reports [6,58–61] and some of their results have indicated that the activity of metal complexes had been often slightly lower than the activity of free quinolones [59,62–64].

Moreover, the antibacterial activities of the compounds were evaluated on *E. coli* and *S. aureus* by the means of disc diffusion method on Mueller-Hinton agar (MHA) at concentrations of 4, 8, 16, 32, and 64 μg/mL. In the disc diffusion method, the diameters of inhibition zones (DIZ) were measured in millimetres (mm) (Fig. 8, Table 8). According to the results, the antimicrobial activity of the complex against the two microorganisms is much higher than that of the metal salt, while being comparable with that of the Hoflo. The complex exhibited equal activity towards Hoflo ligand against *E. coli* (at 4 and 64 μg/mL) and *S. aureus* (at 32 and 64 μg/mL). Based on the measured inhibition zone values (Fig. 8, Table 8), the complex and Hoflo ligand are clearly more active against Gram-negative bacteria while Gram-positive bacteria are more resistant. These observations can be explained by the fact that Gram-negative bacteria are surrounded by a thin peptidoglycan cell wall, which itself is surrounded by an outer membrane containing lipopolysaccharide. On the other hand, Gram-positive bacteria lack an outer membrane but are surrounded by layers of peptidoglycan that is reported to be much thicker than that of the Gram-negatives. The thickness of the cell wall increases the susceptibility of the Gram-positive bacteria to the complex and Hoflo ligand [65–67].

4. Conclusion

In this work, we reported a new ionic oxidovanadium complex, $[VO(Hoflo^z)_2(H_2O)][V_4O_{12}]_{0.5}.6H_2O$ (**1**) that contains antibacterial drug ofloxacin and cyclic tetravanadate anion. This complex was synthesized through the reaction of $VOSO_4$ with ofloxacin ($Hoflo^z$) in presence of KOH with 1:1:1 ratio. In addition, spectral, structural, thermal, biological and molecular docking studies of **1** were investigated as well. In the case of cationic moiety of **1**, the ofloxacin acts as a bidentate ligand in its zwitterionic form through the oxygen atoms of the pyridone and carboxylate groups. In addition to two $Hoflo^z$ ligands, the octahedral geometry of vanadium is completed by coordination of water and an oxo ligand. In the ionic unit, each V^{+5} ion has a tetrahedral geometry. Thermogravimetric analysis of **1** showed that it decomposes in two steps and converts to vanadium(V) oxide.

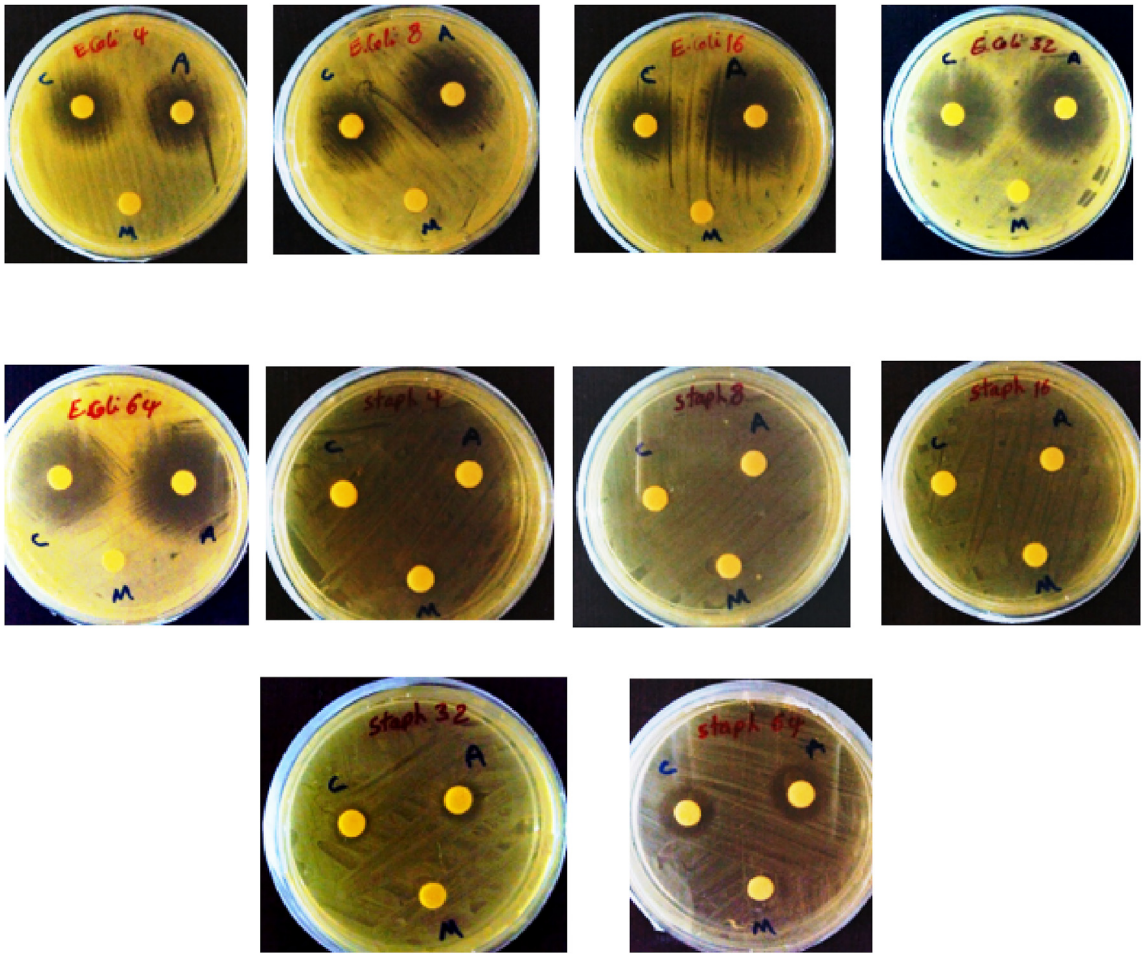

Fig. 8. Shows the antimicrobial activity of $[VO(Hoflo^z)_2(H_2O)][V_4O_{12}]_{0.5}.6H_2O$ complex (C), Hoflo (A) and $VOSO_4$ (M) appear the inhibition zones against pathogenic bacteria (*E.coli* and *S. aureus*).

Table 8
The inhibition diameter zone values (mm) for Hoflo and complex.

Compound	Concentration in DMSO (μg/mL)	The inhibition diameter zone on *E. coli*	The inhibition diameter zone on *S. aureus*
Hoflo	4	24	NA
	8	30	NA
	16	34	NA
	32	33	12
	64	35	15
Complex **1**	4	24	NA
	8	25	NA
	16	26	NA
	32	30	12
	64	35	15

NA: not appearing.

A theoretical study revealed that the aromatic carbon atoms and oxygen atoms of the carboxylate group of $Hoflo^{z}$ along with oxo ligand, have a significant functionality in the electron donation toward V^{+4} ion, as well as in decreasing its charge. Also, the thermodynamic stability of the $Hoflo^{opt}$ is by −87.8 kcal/mol higher than that of the $Hoflo^{z/opt}$. Docking studies revealed that the $Hoflo^{z/opt}$ and $Hoflo^{opt}$ could better interact with CatB, HDAC7 and rHA (only $Hoflo^{opt}$) biomacromolecules than the doxorubicin. Nevertheless, the best-predicted target for $Hoflo^{z/opt}$ and $Hoflo^{opt}$ is HDAC7. The antibacterial activity of the complex has been assayed against *Escherichia coli* (*E. coli*) and *Staphylococcus aureus* (*S. aureus*) strains through the utilization of both microdilution and well diffusion methods. The complex exhibited equal activity to ofloxacin ligand against *E. coli* (at 4 and 64 μg/mL) and *S. aureus* (at 32 and 64 μg/mL), while the results revealed that these compounds were more active against Gram-negative bacteria.

Declaration of competing interests

The authors declare that they have no known competing financial interests or personal relationships that could have appeared to influence the work reported in this paper.

CRediT authorship contribution statement

Mina Alikhani: Methodology, Software, Validation, Investigation, Resources, Data curation, Writing - original draft, Supervision. **Mohammad Hakimi:** Conceptualization, Methodology, Software, Validation, Resources, Writing - original draft, Writing - review & editing, Supervision, Project administration. **Keyvan Moeini:** Software, Validation, Formal analysis, Data curation, Writing - original draft, Writing - review & editing, Visualization. **Mansour Mashreghi:** Software, Validation, Formal analysis, Data curation, Writing - original draft, Writing - review & editing. **Vaclav Eigner:** Software, Formal analysis, Data curation, Writing - review & editing. **Michal Dusek:** Software, Formal analysis, Data curation, Writing - review & editing.

Acknowledgements

We are grateful to the Payame Noor University and the Ferdowsi University of Mashhad for providing the support of this work. The crystallographic part was supported by the project 18-10504 S of the Czech Science Foundation using instruments of the ASTRA laboratory established within the Operation program Prague Competitiveness - project CZ.2.16/3.1.00/24510.

Appendix A. Supplementary data

Supplementary data to this article can be found online at https://doi.org/10.1016/j.molstruc.2020.128300.

References

[1] Y. Mirzaie, J. Lari, H. Vahedi, M. Hakimi, A. Nakhaei, A. Rezaeifard, Fast and green method to synthesis of quinolone carboxylic acid derivatives using giant-Ball nanoporous isopolyoxomolybdate as highly efficient recyclable catalyst in refluxing water, J. Mex. Chem. Soc. 61 (1) (2017) 35–40.
[2] D. Sood, N. Kumar, A. Singh, M.K. Sakharkar, V. Tomar, R. Chandra, Antibacterial and pharmacological evaluation of fluoroquinolones: a chemo-informatics approach, Genomics Inform 16 (3) (2018) 44.
[3] J.L. Zhang, J. Yang, X. Wang, H.Y. Zhang, X.L. Chi, Y. Chen, Q. Yang, D.R. Xiao, Syntheses and structures of two novel interdigitated metal-quinolone complexes:$[Cu_2(cfH)_2(bptc)(H_2O)]\cdot 4H_2O$ and $[Zn_2(levofH)_2(odpa)]\cdot 5.5\ H_2O$, Z. Anorg. Allg. Chem. 641 (5) (2015) 820–825.
[4] A. Debnath, F. Hussain, D.T. Masram, Synthesis, characterization, and antifungal studies of Cr(III) complex of norfloxacin and bipiridyl ligand, J. Inorg. Biochem. 2014 (2014) 1–7.
[5] F.I. Eze, U. Ajali, P.O. Ukoha, Synthesis, physicochemical properties, and antimicrobial studies of iron(III) complexes of ciprofloxacin, cloxacillin, and amoxicillin, Int J Med Chem 2014 (2014), 735602-735602.
[6] V. Uivarosi, Metal complexes of quinolone antibiotics and their applications: an update, Molecules 18 (9) (2013) 11153–11197.
[7] P. Drevenšek, J. Košmrlj, G. Giester, T. Skauge, E. Sletten, K. Sepčić, I. Turel, X-Ray crystallographic, NMR and antimicrobial activity studies of magnesium complexes of fluoroquinolones—racemic ofloxacin and its S-form, levofloxacin, J. Inorg. Biochem. 100 (11) (2006) 1755–1763.
[8] M. Hakimi, M. Alikhani, Characterization of α-Fe_2O_3 nanoparticles prepared from a new $[Fe(Ofloxacin)_2Cl_2]$ precursor: a heterogeneous photocatalyst for removal of methylene Blue and ciprofloxacin in water, J. Inorg. Organomet. Polym. 30 (2) (2020) 504–512.
[9] I. Turel, J. Kljun, F. Perdih, E. Morozova, V. Bakulev, N. Kasyanenko, J.A.W. Byl, N. Osheroff, First ruthenium organometallic complex of antibacterial agent ofloxacin. Crystal structure and interactions with DNA, Inorg. Chem. 49 (23) (2010) 10750–10752.
[10] B. Macias, M.V. Villa, M. Sastre, A. Castiñeiras, J. Borras, Complexes of Co(II) and Zn(II) with ofloxacin. Crystal structure of $[Co(oflo)_2(MeOH)_2]\cdot 4MeOH$, J. Pharm. Sci. 91 (11) (2002) 2416–2423.
[11] B. Macıas, M.a.V. Villa, I. Rubio, A. Castiñeiras, J.n. Borrás, Complexes of Ni(II) and Cu(II) with ofloxacin: crystal structure of a new Cu(II) ofloxacin complex, J. Inorg. Biochem. 84 (3–4) (2001) 163–170.
[12] M.N. Patel, D.S. Gandhi, P.A. Parmar, DNA interaction and in-vitro antibacterial studies of fluoroquinolone based platinum(II) complexes, Inorg. Chem. Commun. 15 (2012) 248–251.
[13] A. Golcu, Ofloxacin metal complexes: synthesis, characterization, analytical properties, and DNA binding studies, Synth. React. Inorg. Metal-Org. Nano-Metal Chem. 44 (10) (2014) 1509–1520.
[14] F. Ahmadi, N. Ebrahimi-Dishabi, K. Mansouri, F. Salimi, Molecular aspect on the interaction of zinc-ofloxacin complex with deoxyribonucleic acid, proposed model for binding and cytotoxicity evaluation, Res Pharm Sci 9 (5) (2014) 367–383.
[15] R.S. Walmsley, Z.R. Tshentu, Imidazole-based vanadium complexes as haloperoxidase models for oxidation reactions, S. Afr. J. Chem. 63 (2010) 95–104.
[16] P.G.A. Martins, M. Mori, L.D. Chiaradia-Delatorre, A.C.O. Menegatti, A. Mascarello, B. Botta, J. Benítez, D. Gambino, H. Terenzi, Exploring oxidovanadium(IV) complexes as YopH inhibitors: mechanism of action and modeling studies, ACS Med. Chem. Lett. 6 (10) (2015) 1035–1040.
[17] A.M.B. Bastos, J.G. da Silva, P.I.d.S. Maia, V.M. Deflon, A.A. Batista, A.V. Ferreira, L.M. Botion, E. Niquet, H. Beraldo, Oxovanadium(IV) and (V) complexes of acetylpyridine-derived semicarbazones exhibit insulin-like activity, Polyhedron 27 (6) (2008) 1787–1794.
[18] Y. Tanabe, Y. Nishibayashi, Recent advances in nitrogen fixation upon vanadium complexes, Coord. Chem. Rev. 381 (2019) 135–150.
[19] A. Bishayee, A. Waghray, M.A. Patel, M. Chatterjee, Vanadium in the detection, prevention and treatment of cancer: the in vivo evidence, Canc. Lett. 294 (1) (2010) 1–12.
[20] J.A. Da Silva, J.J.F. da Silva, A.J. Pombeiro, Oxovanadium complexes in catalytic oxidations, Coord. Chem. Rev. 255 (19–20) (2011) 2232–2248.
[21] R. Bikas, M. Ghorbanloo, S. Jafari, V. Eigner, M. Dusek, Catalytic oxidation of olefins and sulfides in the presence of hydrazone-oxidovanadium(V) complex containing $VOCl_2^+$ core, Inorg. Chim. Acta. 453 (2016) 78–85.
[22] I.S. Fomenko, A.L. Gushchin, P.A. Abramov, M.N. Sokolov, L.S. Shul'pina, N.S. Ikonnikov, M.L. Kuznetsov, A.J. Pombeiro, Y.N. Kozlov, G.B. Shul'pin, New oxidovanadium(IV) complexes with 2, 2′-bipyridine and 1, 10-phenathroline ligands: synthesis, structure and high catalytic activity in oxidations of alkanes and alcohols with peroxides, Catalysts 9 (3) (2019) 217.
[23] M. Sutradhar, L.M.D.R.S. Martins, T. Roy Barman, M.L. Kuznetsov, M.F.C. Guedes da Silva, A.J.L. Pombeiro, Vanadium complexes of different nuclearities in the catalytic oxidation of cyclohexane and cyclohexanol – an experimental and theoretical investigation, New J. Chem. 43 (45) (2019)

17557–17570.
[24] R. Takjoo, A. Akbari, S.Y. Ebrahimipour, M. Kubicki, M. Mohamadi, N. Mollania, Synthesis, spectral characterization, DFT calculations, antimicrobial activity and molecular docking of 4-bromo-2-((2-hydroxy-5-methylphenylimino) methyl)phenol and its V(V) complex, Inorg. Chim. Acta. 455 (2017) 173–182.
[25] Z. Mardani, V. Golsanamlou, Z. Jabbarzadeh, K. Moeini, S. Khodavandegar, C. Carpenter-Warren, A.M. Slawin, J.D. Woollins, Structural conversion of an oxazolidine ligand upon treatment with copper(I) and (II) halides; structural, spectral, theoretical and docking studies, J. Coord. Chem. 71 (24) (2018) 4109–4131.
[26] M. Hakimi, S. Ahmadi, Z. Mardani, F. Mohr, Docking studies on an N4-donor Schiff base ligand and its Cu(II) complex supported by structural, spectral and theoretical studies, J. Chem. Res. 43 (5–6) (2019) 170–178.
[27] Z. Mardani, M. Hakimi, K. Moeini, F. Mohr, Reaction of 2-[(2-aminoethyl) amino] ethanol with pyridine-2-carbaldehyde and complexation of the products with CuII and CdII along with docking studies, Acta Crystallogr. C 75 (7) (2019).
[28] Z. Mardani, R. Kazemshoar-Duzduzani, K. Moeini, A. Hajabbas-Farshchi, C. Carpenter-Warren, A.M. Slawin, J.D. Woollins, Anticancer activities of a β-amino alcohol ligand and nanoparticles of its copper(ii) and zinc(ii) complexes evaluated by experimental and theoretical methods, RSC Adv. 8 (50) (2018) 28810–28824.
[29] L. Saghatforoush, K. Moeini, S.A. Hosseini-Yazdi, Z. Mardani, A. Hajabbas-Farshchi, H.T. Jameson, S.G. Telfer, J.D. Woollins, Theoretical and experimental investigation of anticancer activities of an acyclic and symmetrical compartmental Schiff base ligand and its Co(ii), Cu(ii) and Zn(ii) complexes, RSC Adv. 8 (62) (2018) 35625–35639.
[30] A.A. Adeniyi, P.A. Ajibade, Comparing the suitability of autodock, gold and glide for the docking and predicting the possible targets of Ru(II)-based complexes as anticancer agents, Molecules 18 (4) (2013) 3760–3778.
[31] N.H. Moghadam, S. Salehzadeh, N. Shahabadi, Spectroscopic and molecular docking studies on the interaction of antiviral drug nevirapine with calf thymus DNA, Nucleos. Nusleot. Nucl. 36 (9) (2017) 553–570.
[32] L. Palatinus, G. Chapuis, SUPERFLIP–a computer program for the solution of crystal structures by charge flipping in arbitrary dimensions, J. Appl. Crystallogr. 40 (4) (2007) 786–790.
[33] V. Petříček, M. Dušek, L. Palatinus, Crystallographic computing system JANA2006: general features, Z. für Kristallogr. - Cryst. Mater. 229 (5) (2014) 345–352.
[34] J. Rohlíček, M. Hušák, MCE2005–a new version of a program for fast interactive visualization of electron and similar density maps optimized for small molecules, J. Appl. Crystallogr. 40 (3) (2007) 600–601.
[35] L.E. Budd, R.M. Ibberson, W.G. Marshall, S. Parsons, The effect of temperature and pressure on the crystal structure of piperidine, Chem. Cent. J. 9 (2015), 18-18.
[36] R.A. Gaussian09, 1, mj frisch, gw trucks, hb schlegel, ge scuseria, ma robb, jr cheeseman, g. Scalmani, v. Barone, b. Mennucci, ga petersson et al vol. 121, gaussian, Inc., Wallingford CT, USA, 2009, pp. 150–166.
[37] J.P. Perdew, Density-functional approximation for the correlation energy of the inhomogeneous electron gas, Phys. Rev. B 33 (12) (1986) 8822.
[38] A.D. Becke, Density-functional thermochemistry. III. The role of exact exchange, J. Chem. Phys. 98 (7) (1993) 5648–5652.
[39] R. Ditchfield, W.J. Hehre, J.A. Pople, Self-consistent molecular-orbital methods. IX. An extended Gaussian-type basis for molecular-orbital studies of organic molecules, J. Chem. Phys. 54 (2) (1971) 724–728.
[40] P.J. Hay, W.R. Wadt, Ab initio effective core potentials for molecular calculations. Potentials for the transition metal atoms Sc to Hg, J. Chem. Phys. 82 (1) (1985) 270–283.
[41] A. Gavezzotti, Are crystal structures predictable? Acc. Chem. Res. 27 (10) (1994) 309–314.
[42] G. Jones, P. Willett, R.C. Glen, A.R. Leach, R. Taylor, Development and validation of a genetic algorithm for flexible docking, J. Mol. Biol. 267 (3) (1997) 727–748.
[43] M. Antonijević-Nikolić, J. Antić-Stanković, B. Dražić, S. Tanasković, New macrocyclic Cu(II) complex with bridge terephthalate: synthesis, spectral properties, in vitro cytotoxic and antimicrobial activity. Comparison with related complexes, J. Mol. Struct. 1184 (2019) 41–48.
[44] M. Alikhani, M. Hakimi, K. Moeini, V. Eigner, M. Dusek, Synthesis, characterization and thermal studies of a nanosized 1D l-arginine/copper(II) coordination polymer by sonochemical method: a new precursor for preparation of copper(II) oxide nanoparticles, J. Inorg. Organomet. Polym. Mater. (2020) 1–9.
[45] H. Farrokhpour, H. Hadadzadeh, F. Darabi, F. Abyar, H.A. Rudbari, T. Ahmadi-Bagheri, A rare dihydroxo copper(II) complex with ciprofloxacin; a combined experimental and ONIOM computational study of the interaction of the complex with DNA and BSA, RSC Adv. 4 (67) (2014) 35390–35404.
[46] G. Psomas, D.P. Kessissoglou, Quinolones and non-steroidal anti-inflammatory drugs interacting with copper(II), nickel(II), cobalt(II) and zinc(II): structural features, biological evaluation and perspectives, Dalton Trans. 42 (18) (2013) 6252–6276.
[47] W.-Y. Huang, J. Li, S.-L. Kong, Z.-C. Wang, H.-L. Zhu, Cu(II) and Co(II) ternary complexes of quinolone antimicrobial drug enoxacin and levofloxacin: structure and biological evaluation, RSC Adv. 4 (66) (2014) 35193–35204.
[48] V. Paredes-García, S. Gaune, M. Saldías, M.T. Garland, R. Baggio, A. Vega, M.S. El Fallah, A. Escuer, E. Le Fur, D. Venegas-Yazigi, Solvatomorphs of dimeric transition metal complexes based on the V_4O_{12} cyclic anion as building block: crystalline packing and magnetic properties, Inorg. Chim. Acta. 361 (12–13) (2008) 3681–3689.
[49] A.A. Nejo, G.A. Kolawole, A.R. Opoku, J. Wolowska, P. O'Brien, Synthesis, characterization and preliminary insulin-enhancing studies of symmetrical tetradentate Schiff base complexes of oxovanadium(IV), Inorg. Chim. Acta. 362 (11) (2009) 3993–4001.
[50] M. Hakimi, Z. Mardani, K. Moeini, E. Schuh, F. Mohr, A spectral and structural study of the new cadmium salt $[(H_2L)_2][Cd_2I_6][(NO_3)_2]$, Z. Naturforsch. B Chem. Sci. 68 (3) (2013) 272–276.
[51] M. Hakimi, Z. Mardani, K. Moeini, E. Schuh, F. Mohr, Complexation to cadmium(II) of a tetradentate ligand resulting from the condensation of 2-pyridinecarbaldehyde with N-(2-Aminoethyl) propane-1, 3-diamine, Z. Naturforsch. B Chem. Sci. 68 (3) (2013) 267–271.
[52] F.H. Allen, The Cambridge Structural Database: a quarter of a million crystal structures and rising, Acta Crystallogr. B 58 (3) (2002) 380–388.
[53] S. Mahapatra, K. Venugopala, T.N. Guru Row, A device to crystallize organic solids: structure of ciprofloxacin, midazolam, and ofloxacin as targets, Cryst. Growth Des. 10 (4) (2010) 1866–1870.
[54] S.S. Singh, T.S. Thakur, New crystalline salt forms of levofloxacin: conformational analysis and attempts towards the crystal structure prediction of the anhydrous form, CrystEngComm 16 (20) (2014) 4215–4230.
[55] L.-C. Yu, L. Lai, R. Xia, S.-L. Liu, Syntheses and crystal structures of Zn(II) and Co(II) complexes with ofloxacin and enoxacin, J. Coord. Chem. 62 (8) (2009) 1313–1319.
[56] A.A. Adeniyi, P.A. Ajibade, Comparing the suitability of autodock, gold and glide for the docking and predicting the possible targets of Ru(II)-based complexes as anticancer agents, Molecules 18 (4) (2013) 3760–3778.
[57] N.S. Pagadala, K. Syed, J. Tuszynski, Software for molecular docking: a review, Biophys Rev 9 (2) (2017) 91–102.
[58] M. Hakimi, M. Alikhani, M. Mashreghi, N. Feizi, H. Raeisi, Y. Mirzai, V. Eigner, M. Dusek, A heterodinuclear complex of sd block containing sodium(I), manganese(II) and the enrofloxacinate anion: preparation, crystal structure and antibacterial activity, J. Mol. Struct. 1186 (2019) 355–361.
[59] I. Turel, A. Golobič, A. Klavžar, B. Pihlar, P. Buglyo, E. Tolis, D. Rehder, K. Sepčić, Interactions of oxovanadium(IV) and the quinolone family member—ciprofloxacin, J. Inorg. Biochem. 95 (2–3) (2003) 199–207.
[60] S.M.A. El-Hamid, S.A. Sadeek, W.A. Zordok, W.H. El-Shwiniy, Synthesis, spectroscopic studies, DFT calculations, cytotoxicity and antimicrobial activity of some metal complexes with ofloxacin and 2, 2′-bipyridine, J. Mol. Struct. 1176 (2019) 422–433.
[61] S.A. Sadeek, W.H. El-Shwiniy, Preparation, structure and microbial evaluation of metal complexes of the second generation quinolone antibacterial drug lomefloxacin, J. Mol. Struct. 981 (1) (2010) 130–138.
[62] P. Drevensek, A. Golobic, I. Turel, N. Poklar, K. Sepcic, Crystal structure, characterisation and biological activity of copper(II)-ciprofloxacin ionic compound, Acta Chim. Slov. 49 (2002) 857–870.
[63] L.-C. Yu, Z.-F. Chen, H. Liang, C.-S. Zhou, H.-K. Fun, Hydrothermal synthesis, crystal structure and antibacterial studies of nickel(II) and manganese(II) complexes with ciprofloxacin, J. Coord. Chem. 59 (2006) 953–959.
[64] I. Turel, A. Sonc, M. Zupancic, K. Sepcić, T. Turk, Biological activity of some magnesium(II) complexes of quinolones, Met Based Drugs 7 (2) (2000) 101–104.
[65] T.J. Silhavy, D. Kahne, S. Walker, The bacterial cell envelope, CSH PERSPECT BIOL 2 (5) (2010) a000414.
[66] Y.N. Slavin, J. Asnis, U.O. Häfeli, H. Bach, Metal nanoparticles: understanding the mechanisms behind antibacterial activity, J. Nanobiotechnol. 15 (1) (2017), 65-65.
[67] G.K. Auer, D.B. Weibel, Bacterial cell mechanics, Biochemistry 56 (29) (2017) 3710–3724.